Lipid Corona Formation from Nanoparticle Interactions with Bilayers

Laura L. Olenick, ¹ Julianne M. Troiano, ¹ Ariane Vartanian, ² Eric S. Melby, ^{3,4} Arielle C. Mensch, ⁵ Leili Zhang, ⁵ Jiewei Hong, ⁵ Oluwaseun Mesele, ⁶ Tian Qiu, ⁷ Jared Bozich, ⁸ Samuel Lohse, ⁹ Xi Zhang, ² Thomas R. Kuech, ⁴ Augusto Millevolte, ⁴ Ian Gunsolus, ^{7,10} Alicia C. McGeachy, ¹ Merve Doğangün, ¹ Tianzhe Li, ¹ Dehong Hu, ³ Stephanie R. Walter, ¹ Aurash Mohaimani, ⁸ Angela Schmoldt, ⁸ Marco D. Torelli, ⁵ Katherine R. Hurley, ⁷ Joe Dalluge, ⁷ Gene Chong, ¹¹ Z. Vivian Feng, ¹² Christy L. Haynes, ⁷ Robert J. Hamers, ⁴ Joel A. Pedersen, ^{4,5} Qiang Cui, ^{4,6} Rigoberto Hernandez, ¹¹ Rebecca Klaper, ⁸ Galya Orr, ³ Catherine J. Murphy, ² and Franz M. Geiger¹

¹Department of Chemistry, Northwestern University, Evanston, IL, 60208; ²Department of Chemistry, University of Illinois at Urbana-Champaign, Urbana, IL, 61801; ³Environmental Molecular Sciences Laboratory, Pacific Northwest National Laboratory, Richland, WA 99354; ⁴Environmental Chemistry and Technology Program, University of Wisconsin-Madison, Madison, WI, 53706; ⁵Department of Chemistry, University of Wisconsin-Madison, Madison, WI, 53706; 21218; ⁶Department of Chemistry, Boston University, 590 Commonwealth Avenue, Boston, MA 02215; ⁷Department of Chemistry, University of Minnesota, Minneapolis, Minnesota 55455; ⁸School of Freshwater Sciences, University of Wisconsin-Milwaukee, 600 East Greenfield Avenue, Milwaukee, WI 53204; ⁹Department of Chemistry, Colorado Mesa University, Grand Junction, CO 81501; ¹⁰now at Hennepin County Medical Center, Minneapolis, MN, 55415; ¹¹Department of Chemistry, Johns Hopkins University, Baltimore, MD 21218; ¹²Chemistry Department, Augsburg College, Minneapolis, MN 55454, USA

*Correspondence and requests for materials should be addressed to Franz Geiger
The lead Contact's email address is geigerf@chem.northwestern.edu

SUMMARY.

While mixing nanoparticles with certain biological molecules can result in coronas that afford some control over how engineered nanomaterials interact with living systems, corona formation mechanisms remain enigmatic. Here, we report results from experiments and computer simulations that provide concrete lines of evidence for spontaneous lipid corona formation without active mixing upon attachment to stationary and suspended lipid bilayer membranes. Experiments show that polycation-wrapped particles disrupt the tails of zwitterionic lipids, increase bilayer fluidity, and leave the membrane with reduced ζ-potentials. Computer simulations suggest that the contact ion pairing between the lipid head groups and the polycations' ammonium groups leads to the formation of stable, albeit fragmented, lipid bilayer coronas. The mechanistic insight regarding lipid corona formation can be used for improved control over nano-bio interactions and to help understand why some nanomaterial/ligand combinations are detrimental to organisms while others are not.

138 of 150 Max

KEYWORDS: Nano-bio interface, sustainability, mechanisms of nanoparticle-specific toxicology.

INTRODUCTION.

The propensity of biological species to form coronas around nanoparticles¹⁻⁵ has been used for preparing engineered nanomaterials that can be distributed in biological systems with some control.⁶⁻¹¹ While protein coronas in particular have been studied extensively, ^{1-3,6,7} our understanding of lipid coronas is now just beginning to emerge, ¹²⁻¹⁵ especially of those formed upon unintended nanoparticle contacts with living cells. The protein and lipid corona formation mechanisms appear to differ substantially, as "hard" and "soft" coronas ¹⁶, typical for the former, have not been described for the latter. While pulmonary surfactants can lead to lipid corona formation, ^{3,17-19} it is unclear whether the process can also occur in the more

general case of lipid bilayers, which lack the considerable dipole potential carried by their monolayers counterparts.²⁰ Some precedent for lipid corona formation from cellular bilayer membranes exists in the budding of viruses, which do not possess the machinery to produce their own lipids but instead use charged patches on proteins for sheathing their RNA with a membrane scavenged from the host cell membranes.^{21,22} Likewise, computer simulations indicate coronas of certain lipids may be stable on certain particles,²³⁻²⁵ but the roles of specific functionalization patterns or charge remain poorly understood.²⁶

Here, we ask whether lipid coronas can form spontaneously, i.e. without active mixing, around nanoparticles when they interact with immobilized lipid bilayer membranes, such as those surrounding cells fixed within the extracellular matrix of a living organism. Instead on a human health focus, where 37 °C is the relevant temperature, we consider somewhat lower temperatures (~ 20 °C) that are closer to soil and aquatic environments relevant for the bottom of the food chain. Our experimental design (see Supplementary Note 1) considers a spectrum of model systems that range from supported to suspended lipid bilayers. To test whether corona formation differs for particles having diameters close to or larger than the bilayer thickness, we examine spherical gold metal nanoparticles (AuNPs) having diameters of 4 and 15 nm, chosen as the methods to synthesize, functionalize, and characterize them are well established.²⁷ Complementary experiments using 15-nm diameter nanodiamond particles inform on the generality of the interactions across some varied range of core compositions. We pair our imaging and spectroscopy experiments (see Supplementary Notes 2-4) with molecular dynamics simulations²⁸ of idealized all-atom and coarse-grained models (see Supplementary Notes 5) to probe the lipid corona at an unprecedented level of detail. We then discuss our findings in the context of mitochondriaspecific third-generation sequencing data obtained after exposing the water flea Daphnia

magna, chosen as a well-characterized eukaryote, to the same particle formulations used in our bilayer and bacterial models.

Our study focuses largely on particles wrapped in the cationic encapsulation polyelectrolyte poly(allylamine hydrochloride) (PAH). Particles functionalized with the anionic ligand mercaptopropionic acid (MPA) are probed as well but show generally little interaction with bilayers and biological systems surveyed. As assessed by fluorescence, double centrifugation, the method used to prepare the particles used in our vibrational sum frequency generation (SFG) studies, resulted in a fraction of 0.27 ± 0.04 for the free PAH mass concentration when compared to the mass concentration of cationic (PAH-wrapped) AuNPs in solution. Special attention was therefore given to the role of unbound ligands on the systems studied.

Our model systems focus on particle interactions with supported and suspended lipid bilayers composed of the lipid 1,2-dimyristoyl-sn-glycero-3-phosphocholine (DMPC), given the direct relevance of the zwitterionic PC head group to biological membranes. Additional work probed bilayers formed from DMPC mixed with 10% lipids containing negatively charged head groups in the form of 1,2-dimyristoyl-sn-glycero-3-phospho-1'-rac-glycerol (DMPG). These lipids have gel-to-liquid crystalline phase transition temperatures (T_m near 24°C) below those found in warm-blooded organisms. Given our focus on aquatic and soil environments, where T<T_m, our models allow us to probe how engineered nanomaterials interact with membranes in their solid, i.e. gel, phase. Our choice is also motivated by the fact that PC and PG lipid from pulmonary surfactant monolayers have been reported to be preferentially taken up by carboxylated carbon nanotubes in pulmonary exposure routes. Other lipid combinations we investigated did not show the effects reported herein.

RESULTS AND DISCUSSION.

Lipid tail disruption in zwitterionic lipid bilayers. Vibrational SFG spectra of lipid bilayers report on molecular structure and order within them,³⁵⁻³⁷ in our case the molecular environment of the lipid's C–H oscillators. Indeed, the lipid alkyl tails within the supported bilayers produce strong signals (Fig. 1a, top spectrum) near 2870, 2920, and 2970 cm⁻¹, consistent with the presence of well-formed bilayers. In contrast, the ligands on the AuNPs used in this study are spectroscopically silent (see Supplementary Section 2C), indicating they are likely to be highly disordered under our experimental conditions.

Following exposure of the bilayer at 21±1 °C to 10 nM solutions of the 4-nm sized anionic gold particles, we find only negligible changes in the spectral lineshapes and intensities (Fig. 1a, bottom spectrum). In contrast, exposure of the supported lipid bilayers to the cationic particles coincides with the vanishing of the sharp vibrational features from the lipids (Fig. 1b). A new, spectrally broad signal is observed that is reminiscent of non-resonant sum frequency responses produced by thin gold films, ³⁸ albeit with much smaller intensities, indicating the presence of gold cores at the interface. This outcome is observed for particle concentrations as low as 1 nM. Experiments using bilayers formed from pure DMPC (2a) indicate negatively charged DMPG lipids are not necessarily needed to promote the effect. Moreover, the outcome appears to be invariant with particle size or core type over the range surveyed, as PAH-wrapped 15-nm sized gold and nanodiamond particles show qualitatively the same result (Fig. 1c), albeit with a smaller response from the gold cores than for the 4-nm sized AuNPs. This outcome is consistent with the fourfold smaller mass gain for the larger vs. the smaller particles (vide infra).

Controls (see Supplementary Figures 2b and 2c) indicate the loss of bilayer structure and order upon exposure to the cationic particles does not depend on ionic strength within the range investigated here. Likewise, controls using free PAH do not show altered spectral

responses from the bilayer unless PAH is present in a 100-fold excess over the nanoparticle concentrations employed (Fig. 1d). Other free polycations surveyed also disrupt bilayer structure at comparably high cation concentrations (Supplementary Fig. 2d and 2e).

High coverage of cationic nanoparticles. To quantify the amount of cationic AuNPs on the membranes, we applied quartz crystal microbalance with dissipation (QCMD) monitoring to estimate mass gains (Fig. 2a) and resonantly enhanced second harmonic generation (SHG) measurements to specifically probe the gold cores (Fig. 2b). Mass gains were not detectable above the ~2 ng·cm⁻² limit of detection of the instrument for the anionic particles interacting with supported lipid bilayers rich in DMPC. This outcome is consistent with result reported for supported lipid bilayers formed from pure DOPC³³ as well as pure POPC³⁴ exposed to MPA-functionalized AuNPs. Yet, the SHG measurements provided evidence for the presence of some particles,³⁹ albeit presumably at much smaller surface coverages than what is observed for the cationic particles. We conclude that the 4-nm sized anionic particles interact weakly, if at all, with the bilayers studied under these experimental conditions.

In contrast to the anionic particles, the QCM-D experiments revealed considerable acoustic mass gains when the bilayers were exposed to cationic AuNPs (Fig. 2a). Attributing the surface mass gain solely to the AuNPs, this mass would correspond to roughly $1.9 (\pm 0.2) \times 10^{12}$ particles·cm⁻². Because the acoustic mass includes hydrodynamically coupled solvent, the number of particles per cm² may be less. As shown in Supplementary Fig. 5, the 15-nm diameter cationic particles led to mass gains corresponding to $5.0 (\pm 0.4) \times 10^{11}$ particles·cm⁻² if the acoustic mass were attributed solely to the nanoparticles. Rinsing the supported lipid bilayers with nanoparticle-free solution after attachment of PAH-AuNPs resulted in decreases in energy dissipation and small decreases in mass, which may indicate release of PAH-AuNPs, a small fraction of the bilayer, or some combination of the two, from the surface (see Supplementary Fig. 5).

These results, together with the spectroscopic observations presented earlier, point towards an interaction mechanism that is specific to a combination of bilayer membranes containing lipids having transition temperatures close to room temperature and nm-sized nanoparticles wrapped with polycations, as opposed to with just the free polymer wrapping. Nanoparticles leaving the membrane carry a lower ζ -potential. Motivated by the lines of evidence pointing to the association of membrane lipids with the cationic nanoparticles, we proceeded to collect 4- and 15-nm core PAH-AuNPs after interacting them with the supported lipid bilayers prepared from a 9:1 mix of DMPC:DMPG, measured their electrophoretic mobilities, and calculated their apparent ζ-potentials using the Smoluchowski approximation. PAH-AuNPs that had passed over bare SiO₂-coated sensors were used as controls. Fig. 2c shows the ζ-potentials of the 4- and 15-nm cationic particles measured in the eluent of the QCM-D flow cell (100 mM salt, pH 7.4, 10 mM Tris buffer) decreased from $+32 \pm 2$ mV and $+36 \pm 1$ mV, respectively, in the absence of lipids, to $+24 \pm 2$ mV and $+26 \pm 1$ 1 mV, respectively, upon rinsing from the supported lipid bilayers. These results are consistent with the notion that the nanoparticles collected following interaction with the supported lipid bilayer acquired negatively charged species, likely DMPG, as further supported by calculations (vide infra).

Nanoparticles increase bilayer fluidity 3-4 fold. Single molecule fluorescence microscopy, which we used to track the trajectories of individual phospholipid molecules (Fig. 3a-b), showed a significant increase in the local diffusion coefficients of individual lipids, from an average of 0.0095 ± 0.0062 to $0.035 \pm 0.011 \, \mu m^2 \, s^{-1}$, after interaction with the cationic particles (p < 0.001, Kruskal-Wallis H test with Dunn's *post hoc* test). The value of the lateral diffusion coefficient before interaction with the cationic particles is slightly smaller than those previously reported for gel-phase DMPC bilayers supported on glass, perhaps due to the bilayers being formed via the vesicle fusion method.⁴⁰ A histogram analysis shows that

the average diffusion coefficients increase substantially because of the presence of a large new lipid population, possibly co-localized with the bound particles, that is distinct from the one having coefficients equivalent to the control (Fig. 3c).

The observed increase in the molecular diffusion coefficients indicates an increase in the local fluidity of the gel-phase 9:1 DMPC:DMPG bilayer. We rationalize this outcome by the change in the tilt angle of the electric dipole of the choline headgroup induced by interaction with a cationic amine in the coating⁴¹, increasing the area per lipid head group and thereby decreasing lipid packing density. This interaction represents an initial step in the process of lipid extraction. Removal of lipids from the bilayer would increase the free area per lipid in the remaining bilayer⁴², consistent with the observed increase in diffusivity.

Molecular dynamics simulations reveal stable bilayers forming on nanoparticles wrapped in cationic polyelectrolytes but not on anionic nanoparticles. A lipid corona was seen to form in a coarse-grained simulation (Fig. 4a) providing molecular-level information regarding its structure and composition (Fig. 4b-c). The structure of the coarse-grained PAH-AuNP was validated using sub-microsecond long all-atom simulations of 200-monomer long PAH around an AuNP (see Supplementary Fig. 9). Microsecond-long coarse-grained simulations show significant bilayer bending upon nanoparticle attachment (see Supplementary Note V and Supplementary Fig. 10-13). Given that potential of mean force calculations show lipid extraction by PAH models to be associated with a significant free energy penalty for both zwitterionic and anionic lipids (see Supplementary Fig. 14), the full extraction process of multiple lipids for an entire PAH-wrapped particle interacting with the bilayer is a rare event that is difficult to sample or observe in trajectories even as long as multiple microseconds. Instead, we explored the structure of lipid corona formation by starting from a random distribution around a PAH-wrapped 4-nm sized gold particle; as a control, self-assembly simulations were also conducted with the same gold particle

functionalized with anionic ligands that mimic the MPA. The lipids quickly assemble into micelles but do not attach to the anionic nanoparticle in independent microsecond scale simulations (see Supplementary Fig. 15), supporting the experimental observation that MPA functionalized nanoparticle does not interact significantly with the lipid bilayer. By contrast, in the presence of the PAH-wrapped nanoparticles, the lipid molecules are observed to quickly self-assemble into ribbons and micelles, which then attach to the nanoparticle during ~100 ns (see Supplementary Fig. 16). This result is comparable to what has been reported for the hypothetical case of a bare (ligand free) gold particle interacting with DPPC.²⁵ Unlike in that work, we find here that the lipid bilayer is not uniformly distributed around the particle but instead patchy, which is consistent with the significant bending penalty associated with the lipid membrane around a small (4nm diameter) nanoparticle. For larger nanoparticles (e.g., 15 nm diameter), due to reduced membrane bending penalty, it is likely that more uniform membrane wrapping is stable.²⁴ An analysis of ion/lipid distributions around the nanoparticle indicates that the cationic PAH polymer plays the key role of attracting lipids by contact ion pairing between the ammonium groups and phosphate and glycerol groups (Supplementary Tables 1 and 2). Besides DMPC, the positive charges also recruit anionic lipids (DMPG), leading to a higher fraction of DMPG (32% and 43% for the two simulated systems, respectively) in the lipid corona when compared to the bulk concentration (10%). The dimensionality of the lipid corona model is consistent with observations from our electron microscopy analysis and measured changes in the hydrodynamic radii of the PAHwrapped nanoparticles following corona formation described below.

Nanoparticle-vesicle suspensions form aggregated superstructures featuring lipid headgroup association with particle wrapping moieties. To investigate whether the cationic AuNPs also interact with suspended, as opposed to supported, lipid bilayers, we exposed suspended vesicles to PAH-AuNPs. ¹H NMR spectra of vesicles formed from a 9:1

mixture of DMPC and DMPG show that the ammonium headgroup protons (-N-CH₃, 3.16 ppm) disappear upon addition of 4 nm PAH-AuNPs (Fig. 5a). The hydrocarbon proton resonances are broadened beyond detection because the lipids exist in the lipid ordered phase at the laboratory temperature at which the experiment was run (20 °C, below the transition temperatures of DMPC (24 °C) and DMPG (23 °C)). The disappearance of the headgroup proton resonance can best be explained by attachment of the headgroup to another species, presumably PAH, which would immobilize the protons and broaden the resonance into the baseline. Indeed, the PAH-AuNP protons shift significantly upfield after interaction with the lipid vesicles, suggesting that the PAH layer is now sandwiched between the gold surface and an additional species. Taken together, the NMR data support the conclusions from the supported lipid bilayer studies that lipids strongly associate with the surface of the cationic AuNPs.

Additional experiments using dynamic light scattering and fluorescence microscopy of the nanoparticle-vesicle suspensions reveal the formation of aggregated superstructures: the hydrodynamic diameters of the vesicles double upon addition of the cationic particles to 200 ± 10 nm and further increase in the subsequent two hours to >1 µm. Spinning disk confocal fluorescence microscopy experiments show the rapid build-up of sub- and super-µm-sized agglomerates that are immobilized at the solution/glass interface of the imaging cell (Fig. 5b), indicating the newly formed structures are considerably stickier than the PAH-wrapped nanoparticles or the lipid vesicles themselves. These microscopy images also show that the particles that produce fluorescence signals have the labels far enough from the gold core that the fluorescence is not quenched. Yet, we find that many of the fluorescent features are seemingly co-localized with similarly sized features observed in the bright field (Supplementary Fig. 8), which visualizes particles that are agglomerated to mm-sized structures. This effect is seen for many of the sub-micron sized features. These features are

not formed when PAH-wrapped nanoparticles are brought in contact with vesicles formed from a 9:1 mix of DOPC and DOTAP (Supplementary Fig. 6), when 9:1 DMPC:DMPG vesicles are exposed to 10 nM free PAH, or when 9:1 DMPC:DMPG vesicles are brought in contact with anionic, MPA-functionalized AuNPs (Supplementary Figure 7).

Our work presents unprecedented views of lipid coronas forming spontaneously when lipid bilayers are brought into contact with cationic nanoparticles. As summarized in Table I, lipid coronas were shown to form spontaneously when polycation-wrapped 4- and 15-nm diameter nanoparticles, be their cores made of gold or nanodiamond, interact with a variety of bilayer membranes, be they immobilized or suspended. By pairing spectroscopic and imaging experiments with atomistic and coarse-grain simulations on idealized model systems, we identify contact ion pair formation between the ammonium groups of the polycationic nanoparticle wrapping and the negatively charged lipid head group moieties as a key formation mechanism for lipid coronas. By paying careful attention to free ligand controls, we identified particle-specific effects that require 100 times smaller N⁺ concentrations than what was needed to promote membrane disruption using just the bare ligands.

Taken together, the results described above provide several concrete, as opposed to hypothetical, lines of evidence regarding nanoparticle-lipid interactions that may help us understand and predict, from a molecular level, why some nanomaterial/ligand combinations are detrimental to cellular organisms while others are not. How the original state, identity, and composition of the lipids in a given membrane determines whether a lipid corona may form is an open question that needs to be addressed. Indeed, we caution that the implications of our results are limited to the nanoparticle formulations and lipid compositions surveyed here. We realize that an intervening protein corona layer may also impact lipid corona formation. ^{33,43} Indeed, we have demonstrated in related experiments that the presence of certain proteins in certain nanoparticle coronas can coincide with the adsorption of

nanoparticles to lipid bilayers that would otherwise not occur.³³ Future work will address the interplay between proteins and lipids in biomolecular coronas, including competitive exchange between the functional groups of nanoparticle coatings or wrappings and lipids vs. proteins. Yet, even on its own, lipid corona formation may also be critically important in more complex biological systems if the corona-forming structures require the presence of lipid-specific functional groups, such as phosphate (as shown here through ammonium-phosphate contact ion pair formation), that are absent or considerably less abundant in proteins.

The results presented here may be of relevance for explaining the molecular origin of nanoparticle-specific and dose-dependent decreases in the viability of *Shewanella*⁴⁴ and *Daphnia*^{45,46} exposed to the same nanoparticle formulations (ligands and size and core composition) for which lipid corona formation is reported here. Ongoing efforts focus, therefore, on uncovering possible links between lipid corona formation and oxidative stress in daphnid tissues⁴⁷ as well as the alteration of the expression of individual genes, in the form of RNA production, specifically those associated with metabolism, reproduction, and growth. In the long term, we believe that our approach for studying the nano-bio interface, in which understanding the nanomaterial and its coating along with the biological membrane is considered equally important, will increase our ability to predict the impact that the increasingly widespread use of engineered nanomaterials in industrial applications and consumer products has on the fate of these materials once they enter the environment and the food chain, which many of them may eventually do. Section 1.

2963 of 3000 Words Max for Intro, Results, Discussion

PROCEDURES.

Materials, nanoparticle synthesis, bilayer preparation, and characterization. The synthesis, functionalization, and characterization of the nanoparticles and bilayers studied

here have been described in our prior work^{32,46} and are discussed in further detail as described in Supplementary Note 1.

Single molecule trajectories. Supported lipid bilayers were formed within 35/22 mm #1.5 glass bottom dishes (Willco Wells). Dishes were rinsed with ultrapure water (18 MΩ·cm; MilliQ Advantage A10, Millipore), dried with N2, and cleaned in a UV/Ozone chamber (PSD Pro Series, Novascan) for 20 min. Cleaned dishes were equilibrated with a solution containing 0.1 M NaCl buffered to pH 7.4 with 0.010 M Tris for at least 1 h. Suspensions of small unilamellar vesicles (SUVs) (0.0625 mg·mL⁻¹ 9:1 DMPC:DMPG with 0.0001 mol% fluorescent Atto 647N DOPE (Atto-Tec; $\lambda_{ex} = 642$ nm; $\lambda_{em} = 667$ nm) in the same buffered solution used to equilibrate the dishes) were introduced to the dish. After bilayer formation, the solution in the dish was exchanged five times with 2 mL aliquots of the buffered solution. Single molecule fluorescence imaging of supported lipid bilayers was conducted before and after introduction of 1 nM PAH-AuNPs. Imaging was conducted on an Olympus IX71 inverted microscope with a UPlanSApo 100× 1.4 NA oil-immersion objective. Fluorescence emission was acquired with an Andor iXon Ultra EMCCD operated at 6.9 Hz. The excitation source was a 643 nm pumped laser (CL-2000, Crystal Laser). A series of at least 500 frames was collected at three spots (250 × 250 pixels, 40 × 40 μm) before and after 1 nM PAH-AuNP addition, and this was repeated on three different supported lipid bilayers. MATLAB (R2015a, MathWorks) was used to determine the trajectories of individual lipid molecules and lateral lipid diffusion coefficients. Individual fluorescent molecules were identified as unique, diffraction limited points with the expected fluorescence intensity of single dye molecules, as predetermined by spin-coating the dye molecules on a glass coverslip and imaging them using the same settings. These points were tracked from one frame to the next to reconstruct the trajectories of individual lipid molecules. The lateral diffusion coefficient, D_L, was determined from the mean squared displacement, MSD, and the time between frames,

t, using the relation $MSD = 4D_Lt$.

Computer Simulations. To understand how lipid corona is formed around gold nanoparticles wrapped with positively charged PAH polymers, we use molecular dynamics simulations with the POL-MARTINI coarse-grained force field. 53,54 The gold nanoparticle is constructed as a 4-nm diameter sphere with fcc lattice structure, where all beads are treated as the C1 type (the most hydrophobic in the MARTINI force field) with 4.7 Å as the van der Waals radius; a similar model for the gold nanoparticle has been employed successfully in previous coarse-grained molecular dynamics simulations of functionalized nanoparticles and their interactions with lipid membranes. 55,56 All beads beyond 1.8 nm from the center of the nanoparticle are assigned with a negative charge of -1, qualitatively mimicking the effect of surface passivation by citric acids; as a result, the Lennard-Jones parameters of the CG gold beads are expected to be less important than in previous CG simulations.⁵⁶ The force field of PAH polymer is established by combining the carbon backbones of polystyrene⁵⁷ and the top bead of the lysine side chain from MARTINI.53 Two PAH models that contain 160 and 200 monomers, respectively, are constructed, since exploratory simulations indicate that these chain lengths lead to a significant degree of surface coverage of the nanoparticle once it is wrapped by the PAH polymer. All monomers are assumed to be positively charged, which likely leads to an overestimated charge of PAH.⁵⁸ The interfacial electrostatic potential of the nanoparticle in salt solution is about +100 mV at the van der Waals surface of the PAH polymer that wraps the gold nanoparticle, thus the z-potential is expected to be substantially lower, in the range of 50 mV, which can be compared to the experimental measured value of +30 mV. 32 Thus, we expect that the current model is appropriate for exploring the qualitative nature of the lipid corona. The calibration of the coarse-grained model using an all-atom representation of the PAH interacting with the gold nanoparticle is described in Supplementary Note 5. We note that while it is possible that more than one PAH polymer is

adsorbed onto the gold nanoparticle, ^{59,60} the current CG model for the PAH wrapped AuNP is sufficient for probing the fundamental interactions that drive the formation of the lipid corona. More detailed analysis of the corona formation mechanism requires further characterization of PAH conformations at the AuNP surface, including the impact of the citrates, which are the subjects of on-going experimental and computational studies. For the MPA functionalized nanoparticle, the MPA ligand is described using the MARTINI model with parameters similar to an aspartate.

To study the organization of lipids near the PAH-wrapped gold nanoparticle, selfassembly simulations are carried out by randomly placing lipids around a gold nanoparticle wrapped with a PAH chain that contains 160 or 200 monomers. The solution contains 423 copies of DMPC molecules and 47 copies of DMPG molecules, and 0.02 M NaCl solution with MARTINI polarizable water model. The dimension of the simulation box is 15×15×15 nm³. The time step of the simulations is 20 fs. Electrostatic interactions are treated with the particle mesh Ewald (PME) method,⁶¹ with a Fourier spacing of 0.12 nm. Van der Waals interactions are treated by the shift scheme, with a cut-off distance of 1.2 nm and the switching function turned on at 0.9 nm. Isothermal-isobaric (NpT) simulations are carried out at 300 K and 1.0 bar using the Berendsen thermostat and pressure coupling (compressibility of 3×10⁻⁵ 1/bar), ⁶² calculations are repeated using the semi-isotropic pressure coupling and the qualitative results remain the same. The system is subject to 20,000 steps of steepest descendant energy minimization before 1 ns of NVT equilibration and 400 ns of production simulations. Several independent simulations are carried out to ensure the robustness of the qualitative trends. For the self-assembly of lipids around a MPA functionalized nanoparticle, the setup is identical, other than the model used for the MPA ligands. For a summary of all simulations conducted, see Supplementary Table 3.

ACKNOWLEDGMENTS. This work was supported by the National Science Foundation

Center for Chemical Innovation Program, through the Center for Sustainable Nanotechnology (CSN) under Grant No. CHE-1503408. JMT and ACM gratefully acknowledge support through an NSF Graduate Research Fellowship. SRW was supported by an Arnold O. Beckman Scholarship of the Chicago chapter of the Achievement Rewards for College Scientists (ARCS) foundation. FMG gratefully acknowledges support from a Friedrich Wilhelm Bessel Prize from the Alexander von Humboldt Foundation. Part of this research was performed using the Environmental Molecular Sciences Laboratory (EMSL), a national scientific user facility sponsored by the Department of Energy's Office of Biological and Environmental Research and located at PNNL. RH acknowledges the National Science Foundation through XSEDE resources provided by Stampede under grant number CTS090079. Additional computing resources were provided by the Maryland Advanced Research Computing Center (MARCC).

AUTHOR CONTRIBUTIONS. LLO, JMT, AV, ESM, SL, TRK, IG, ACM, MD, TL, SRW, SL, HO, MH, MDT, VF, KRH, JD, JB, and GD performed the experiments. LZ, OM, JH, GC, RH, and QC performed the computational work. The data was analyzed and the manuscript was written with substantial contributions from all authors.

DECLARATION OF INTERESTS. The authors declare no competing interests.

SUPPLEMENTAL INFORMATION. Supplementary information accompanies this article online at *URL*, including movie of corona structure and dynamics.

REFERENCES

- 1 Cedervall, T., Lynch, I., Lindman, S., Berggard, T., Thulin, E., Nilsson, H., ... & Linse, S. Understanding the nanoparticle-protein corona using methods to quantify exchange rates and affinities of proteins for nanoparticles. *Proc. Natl. Acad. Sci.* 104, 2050-2055 (2007).
- Liu, J. Q., Zhang, Q., Remsen, E. E. & Wooley, K. L. Nanostructured materials designed for cell binding and transduction. *Biomacromolecules* **2**, 362-368 (2001).
- Docter, D., Westmeier, D., Markiewicz, M., Stolte, S., Knauer, S. K. & Staubert, R. H. The nanoparticle biomolecule corona: lessons learned challenge accepted? *Chem. Soc. Rev.* 44, 6096-6121 (2015).
- Westmeier, D., Stauber, R. H. & Docter, D. The concept of bio-corona in modulating the toxicity of engineered nanomaterials (ENM). *Toxicology and Applied Pharmacology* **299**, 53-57 (2016).

Monopoli, M. P., Aberg, C., Salvati, A. & Dawson, K. A. Biomolecular coronas provide the biological identity of nanosized materials. *Nature Nanotech.* **7**, 779-786 (2012).

- Salvati, A., Pitek, A. S., Monopoli, M. P., Prapainop, K., Bombelli, F. B., Hristov, D. R., ... & Dawson, K. A. Transferrin-functionalized nanoparticles lose their targeting capabilities when a biomolecular corona adsorbs on the surface. *Nature Nanotechnology* **8**, 137-143 (2013).
- Lesniak, A., Fenaroli, F., Monopoli, M. P., Aberg, C., Dawson, K. A. & Salvati, A. Effects of Presence or Absence of a Protein Corona on Silica Nanoparticle Uptake and Impact on Cells. *ACS Nano* 6, 5845-5857 (2012).
- 8 Hellstrand, E., Lynch, I., Andersson, A., Drakenberg, T., Dahlback, B., Dawson, K. A., ... & Cedervall, T. Complete High-Density Lipoproteins in Nanoparticle Corona. *FEBS* **276**, 3372-3381 (2009).
- 9 Guo, Y., Terrazzi, E., Seemann, R., Fleury, J. B. & Baulin, V. A. Direct proof of spontaneous translocation of lipid-covered hydrophobic nanoparticles through a phospholipid bilayer. *Science Advances* 2, e1600261 (2016).
- Xu, F. D., Reiser, M., Yu, X. W., Gummuluru, S., Wetzler, L. & Reinhard, B. M. Lipid-Mediated Targeting with Membrane Wrapped Nanoparticles in the Presence of Corona Formation. *ACS Nano* 10, 1189-1200 (2016).
- Hu, C.-M., Zhang, L., Aryal, S., Cheung, C., Fang, R. H. & Zhang, L. Erythrocyte membrane-camouflaged polymeric nanoparticles as a biomimetic delivery platform. *Proc Natl Acad Sci U S A* **108**, 10980-10985 (2011).
- Bahrami, A. H., Raatz, M., Agudo-Canalejo, J., Michel, R., Curtis, E. M., Hall, C. K., ... & Weikl, T. R. Wrapping of nanoparticles by membranes. *Adv. Colloid Interface Sci.* **208**, 214-224 (2014).
- Zhang, S. L., Gao, H. & Bao, G. Physical Principles of Nanoparticle Cellular Endocytosis. *ACS Nano* **9**, 8655-8671 (2015).
- Amici, A., Caracciolo, G., Digiacomo, L., Gambini, V., Marchini, C., Tilio, M., ... & Lagana, A. In vivo protein corona patterns of lipid nanoparticles. *RSC Advances* 7, 1137-1145 (2017).
- Muller, J.-F., Prozeller, D., Ghazaryan, A., Kokkinopoulou, M., Mailander, V., Morsbach, S. & Landfester, K. Beyond the protein corona lipids matter for biological response of nanocarriers. *Acta Biomat.* 71, 420-431 (2018).
- Milani, S., Bombelli, F. B., Pitek, A. S., Dawson, K. A. & Raedler, J. Reversible Versus Irreversible Binding of Transferrin to Polystyrene Nanoparticles: Soft and Hard Corona. *ACS Nano* 6, 2532-2541 (2012).
- 17 Sachan, A. K., Harishchandra, R. K., Bantz, C., Maskos, M., Reichelt, R. & Galla, H.-J. High-Resolution Investigation of Nanoparticle Interaction with a Model Pulmonary Surfactant Monolayer. *ACS Nano* 2, 1677-1687 (2012).
- Raesch, S. S., Tenzer, S., Storck, W., Rurainski, A., Selzer, D., Ruge, C. A., ... & Lehr, C.-M. Proteomic and Lipidomic Analysis of Nanoparticle Corona upon Contact with Lung Surfactant Reveals Differences in Protein, but Not Lipid Composition. *ACS Nano* 12, 11872-11885 (2015).
- Kapralov, A. A., Feng, W. H., Amoscato, A. A., Yanamala, N., Balasubramanian, K., Winnica, D. E., ... & Kagan, V. E. Adsorption of Surfactant Lipids by Single-Walled Carbon Nanotubes in Mouse Lung upon Pharyngeal Aspiration. *ACS Nano* 6, 4147-4156 (2012).
- Casper, C. B., Verreault, D., Adams, E. M., Hua, W. & Allen, H. C. Surface Potential of DPPC Monolayers on Concentrated Aqueous Salt Solutions. *Journal of Physical Chemistry B* **120**, 2043-2052 (2016).
- Bornholdt, Z. A., Noda, T., Abelson, D. M., Halfmann, P., Wood, M. R., Kawaoka, Y. & Saphire, E. O. Structural Rearrangement of Ebola Virus VP40 Begets Multiple Functions in the Virus Life Cycle. *Cell* **154**, 763-774 (2013).
- Dessen, A., Volchkov, V., Dolnik, O., Klenk, H.-D. & Weissenhorn, W. Crystal structure of the matrix protein VP40 from Ebola virus. *EMBO* **19**, 4228 (2000).
- Hu, M., Stanzione, F., Sum, A. K., Faller, R. & Deserno, M. Design Principles for Nanoparticles Enveloped by a Polymer-Tethered Lipid Membrane. *ACS Nano* **9**, 9942-9954 (2015).

Spangler, E. J., Upreti, S. & Laradji, M. Partial wrapping and spontaneous endocytosis of spherical nanoparticles by tensionless lipid membranes. *J. Chem. Phys.* **144**, 044901 (2016).

- Lai, C.-T., Sun, W., Palekar, R. U., Thaxton, C. S. & Schatz, G. C. Molecular Dynamics Simulation and Experimental Studies of Gold Nanoparticle Templated HDL-like Nanoparticles for Cholesterol Metabolism Therapeutics. *ACS Applied Materials & Interfaces* 9, 1247-1254 (2017).
- Van Lehn, R. C., Ricci, M., Silva, P. H. J., Andreozzi, P., Reguera, J., Voitchovsky, K., ... & Alexander-Katz, A. Lipid tail protrusions mediate the insertion of nanoparticles into model cell membranes. *Nature communications* **5482** (2014).
- Dreaden, E. C., Alkilany, A. M., Huang, X. H., Murphy, C. J. & El-Sayed, M. A. The golden age: gold nanoparticles for biomedicine. *Chem. Soc. Rev.* 41, 2740-2779 (2012).
- Cui, Q., Hernandez, R., Mason, S. E., Fraunheim, T., Pedersen, J. A. & Geiger, F. M. Sustainable Nanotechnology: Opportunities and Challenges for Theoretical/Computational Studies. *J. Phys. Chem. B* **120**, 7297-7306 (2016).
- Qiu, T. A., Torelli, M. D., Vartanian, A. M., Rackstraw, N. B., Jacob, L. M., Buchman, J. T., ... & Haynes, C. L. Quantification of Free Ligands Present in Colloidal Suspension Reveals Source of Toxic Responses for Polyelectrolyte-wrapped 4-nm-diameter Gold Nanoparticles. *Analytical Chemistry* **89**, 1823-1830 (2017).
- Martinez-Morales, F., Schobert, M., Lopez-Lara, I. M. & Geiger, O. Pathways for phosphatidylcholine biosynthesis in bacteria. *Microbiology* **149**, 3461-3471 (2003).
- Geiger, O., López-Lara, I. M. & Sohlenkamp, C. Phosphatidylcholine biosynthesis and function in bacteria. *Biochimica et Biophysica Acta (BBA) Molecular and Cell Biology of Lipids* **1831**, 503-513 (2013).
- Troiano, J., Olenick, L., Kuech, T., Melby, E., Hu, D., Lohse, S., ... & Geiger, F. Direct Probes of 4-nm Diameter Gold Nanoparticles Interacting with Supported Lipid Bilayers. *J. Phys. Chem C* 119, 534-546 (2015).
- Melby, E. S., Lohse, S. E., Park, J. E., Vartanian, A. M., Putans, R. A., Abbott, H. B., ... & Pedersen, J. A. Cascading Effects of Nanoparticle Coatings: Surface Functionalization Dictates the Assemblage of Complexed Proteins and Subsequent Interaction with Model Cell Membranes. *ACS Nano* 11, 5489-5499 (2017).
- Jacobson, K. H., Gunsolus, I. L., Kuech, T. R., Troiano, J. M., Melby, E. S., Lohse, S. E., ... & Pedersen, J. A. Lipopolysaccharide Density and Structure Govern the Extent and Distance of Nanoparticle Interaction with Actual and Model Bacterial Outer Membranes. *Environmental Science & Technology* 49, 10642-10650 (2015).
- Walker, R. A., Conboy, J. C. & Richmond, G. L. Molecular Structure and Ordering of Phospholipids at a Liquid–Liquid Interface. *Langmuir* 13, 3070-3073 (1997).
- Liu, J. & Conboy, J. C. Direct Measurement of the Transbilayer Movement of Phospholipids by Sum-Frequency Vibrational Spectroscopy. *J. Am. Chem. Soc.* **126**, 8376-8377 (2004).
- Olenick, L. L., Chase, H. C., Fu, L., Zhang, Y., McGeachy, A. C., Dogangun, M., ... & Geiger, F. M. Single-Component Supported Lipid Bilayers Probed Using Broadband Nonlinear Optics. *PCCP Advance Article DOI 10.1039/C7CP02549A* (2018).
- Richter, L. J., Petralli-Mallow, T. P. & Stephenson, J. C. Vibrationally resolved sum-frequency generation with broad-bandwidth infrared pulses. *Opt. Lett.* **23**, 1594-1596 (1998).
- Troiano, J. M., Kuech, T. R., Vartanian, A. M., Torelli, M. D., Sen, A., Jacob, L. M., ... & Geiger, F. M. On Electronic and Charge Interference in Second Harmonic Generation Responses from Gold Metal Nanoparticles at Supported Lipid Bilayers. *The Journal of Physical Chemistry C* (2016).
- Scomparin, C., Lecuyer, S., Ferreira, M., Charitat, T. & Tinland, B. Diffusion in supported lipid bilayers: Influence of substrate and preparation technique on the internal dynamics. *Eur. Phys. J. E* **28**, 211-220 (2009).

Wang, B., Zhang, L., Bae, S. C. & Granick, S.Nanoparticle-induced surface reconstruction of phospholipid membranes. Vol. 105 18171-18175 (National Acad Sciences, 2008)

- Vaz, W. L. C., Goodsaid-Zalduondo, F. & Jacobson, K. Lateral diffusion of lipids and proteins in bilayer membranes. *Federation of European Biochemical Societies* **174**, 199-207 (1984).
- Di Silvio, D., Maccarini, M., Parker, R., Mackie, A., Fragneto, G. & Bombelli, F. B. The effect of the protein corona on the interaction between nanoparticles and lipid bilayers. *J. Colloid Interface Sci.* **504**, 741-750 (2017).
- Feng, Z. V., Gunsolus, I. L., Qiu, T. A., Hurley, K. R., Nyberg, L. H., Frew, H., ... & Haynes, C. L. Impacts of gold nanoparticle charge and ligand type on surface binding and toxicity to Gram-negative and Gram-positive bacteria. *Chemical Science* 6, 5186-5196 (2015).
- Qiu, T. A., Bozich, J. S., Lohse, S. E., Vartanian, A. M., Jacob, L. M., Meyer, B. M., ... & Klaper, R. D. Gene expression as an indicator of the molecular response and toxicity in the bacterium Shewanella oneidensis and the water flea Daphnia magna exposed to functionalized gold nanoparticles. *Env. Sci: Nano* 2, 615-629 (2015).
- Bozich, J. S., Lohse, S. E., Torelli, M. D., Murphy, C. J., Hamers, R. J. & Klaper, R. D. Surface chemistry, charge and ligand type impact the toxicity of gold nanoparticles to Daphnia magna. *Environ. Sci.: Nano* 1, 260-270 (2014).
- Dominguez, G. A., Lohse, S. E., Torelli, M. D., Murphy, C. J., Hamers, R. J., Orr, G. & Klaper, R. D. Effects of Charge and Surface Ligand Properties of Nanoparticles on Oxidative Stress and Gene Expression within the Gut of Daphnia Magna. *Aq. Tox.* **162**, 1-9 (2015).
- Nel, A., Xia, T., Mädler, L. & Li, N. Toxic Potential of Materials at the Nanolevel. *Science* 311, 622-627 (2006).
- Maynard, A. D., Aitken, R. J., Butz, T., Colvin, V., Donaldson, K., Oberdorster, G., ... & Warheit, D. B. Safe handling of nanotechnology. *Nature* **444**, 267-269 (2006).
- Lead, J. R. & Smith, E.Envrionmental and Human Health Impacts of Nanotechnology (John Wiley & Sons, United Kingdom, 2009)
- Westerhoff, P. & B., N. Searching for Global Descriptors of Engineered Nanomaterial Fate and Transport in the Environment. *Acc. Chem. Res.* **46**, 844-853 (2013).
- Ferry, J. L., Craig, P., Hexel, C., Sisco, P., Frey, R., Pennington, P. L., ... & Shaw, T. J. Transfer of gold nanoparticles from the water column to the estuarine food web. *Nature Nanotechnology* **4**, 441-444 (2009).
- Marrink, S. J., Risselada, H. J., Yefimov, S., Tieleman, D. P. & Vries, A. H. d. The MARTINI force field: coarse grained model for biomolecular simulations. *J. Phys. Chem. B* 111, 7812-7824 (2007).
- Yesylevskyy, S. O., Schafer, L. V., Sengupta, D. & Marrink, S. J. Polarizable water model for the coarse-grained Martini force field. *PLoS Comp. Biol.* **6**, e1000810 (2010).
- Lehn, R. C. V. & Alexander-Katz, A. Penetration of lipid bilayers by nanoparticles with environmentally-responsive surfaces: simulations and theory. *Soft Matt.* 7, 11392-11404 (2011).
- Ramazani, A., Mandal, T. & Larson, R. G. Modeling the hydrophobicity of nanoparticles and their interaction with lipids and proteins. *Langmuir* **32**, 13084-13094 (2016).
- Rossi, G., Monticelli, L., Puisto, S. R., Vattulainen, I. & Ala-Nissila, T. Coarse-graining polymers with the MARTINI force field: polysteyrene as a benchmark case. *Soft Matt.* 7, 698-708 (2011).
- Troiano, J. M., McGeachy, A. C., Olenick, L. L., Fang, D., Liang, D., Hong, J., ... & Geiger, F. M. Quantifying the Electrostatics of Polycation–Lipid Bilayer Interactions. *J. Am. Chem. Soc.* **139**, 5808-5816 (2017).
- Torelli, M. D., Putans, R. A., Tan, Y. H., Lohse, S. E., Murphy, C. J. & Hamers, R. J. Quantitative determination of ligand densities on nanomaterials by X-ray photoelectron spectroscopy. *ACS Applied Materials & Interfaces* 7, 1720-1725 (2015).

- 61
- Chong, G. & Hernandez, R. Adsorption Dynamics and Structure of Polycations on Citrate-coated Gold Nanoparticles. *Submitted* (2018).

 Frenkel, D. & Smit, B. *Understanding Molecular Simulation: From Algorithms to Applications*. (Academic Press, 2001).

 Berendsen, H. J. C., Postma, J. P. M., van Gunsteren, W. F., Di Nola, A. & Haak, J. R. Molecular dynamics with coupling to an external bath. *J. Chem. Phys.* 81, 3684-3690 (1084). 62 (1984).

LIST OF FIGURES.

Figure 1. Molecular order within lipid bilayers changes upon interaction with PAH-wrapped particles. (a) ssp-Polarized SFG spectra obtained from supported lipid bilayers prepared from a 9:1 mixture of DMPC:DMPG held at 100 mM NaCl and pH 7.4 (10 mM Tris buffer) before (top) and after (bottom) introduction of MPA-coated 4-nm sized gold metal nanoparticles. (b) SFG responses obtained from supported lipid bilayers prepared from a 9:1 mixture of DMPC:DMPG held at 100 mM NaCl and pH 7.4 (10 mM Tris buffer) following exposure to 4-nm sized PAH-wrapped particles at concentrations indicated. (c) SFG responses obtained from supported lipid bilayers prepared from a 9:1 mixture of DMPC:DMPG held at 100 mM NaCl and pH 7.4 (10 mM Tris buffer) following exposure to PAH-wrapped gold and nanodiamond particles having the indicated core diameters. (d) SFG responses obtained from supported lipid bilayers prepared from a 9:1 mixture of DMPC:DMPG held at 100 mM NaCl and pH 7.4 (10 mM Tris buffer) following exposure to free ligand at concentrations indicated. Spectra offset for clarity. See also Supplementary Note 2 and Figures S1 - S2.

Figure 2. PAH-wrapped nanoparticles form large surface coverages on supported lipid bilayers and lower their ζ Potentials. (a) Acoustic mass gains, determined from QCM-D measurements, of 10 nM solutions of PAH-(blue) and MPA-(red) coated 4-nm AuNPs before, during (20 min), and after contact with supported lipid bilayers composed of 9:1 DMPC:DMPG maintained at pH 7.4, 10 mM Tris buffer, and 100 mM salt. (b) Fractional SHG signal gain as a function of concentration of PAH-(blue) and MPA-(red) coated 4-nm AuNPs referenced to the SHG signal intensity obtained from supported lipid bilayer composed of 9:1 DMPC:DMPG maintained at pH 7.4, 10 mM Tris buffer, and 100 mM salt. (c) ζ Potentials of PAH-AuNPs prior to contact with and after rinsing from 9:1 DMPC:DMPG bilayers. Solutions were pH 7.4 (10 mM Tris) and contained 100 mM NaCl.

Error bars indicate one standard error for each point estimate from three replicates. See also Supplementary Note 3 and Figures S3 - S5.

Figure 3. Lipid diffusion is altered by interaction with PAH-wrapped nanoparticles. Trajectories of individual Atto 647N DOPE lipid molecules in a 9:1 DMPC:DMPG bilayer. Reconstructed lipid trajectories before (a) and after (b) the addition of 1 nM PAH-AuNPs. Colors indicate lateral diffusion coefficients [D_L , $\mu m^2 s^{-1}$] for individual lipid molecules. Lateral diffusion coefficients of all labeled lipid molecules (three spots on each bilayer and three bilayer replicates) were averaged to determine the mean lateral diffusion coefficients presented in (e). The error bars correspond to one standard deviation. (c) Histograms of molecular diffusion coefficients shown in (a) and (b) before (green) and after (blue) interaction of bilayers with the PAH-wrapped nanoparticles.

Figure 4. Coarse grain molecular dynamics simulations show stable bilayer membrane fragments surrounding PAH-wrapped nanoparticles. The final snapshot after 400 ns of simulations using the POL-MARTINI coarse-grained model from a self-assembly simulation of lipids corona formation around a gold metal nanoparticle wrapped in a single PAH polymer having 160 monomers (a) and zoomed in view of just the phosphate (orange), PG head group glycerol (red) and choline (green) groups within 6 Å of the cationic side chain of PAH (ice blue/gray) or Au (yellow) (b). Phosphates are colored in dark blue, lipid tails are shown as while/purple lines. Smaller yellow and light blue spheres indicate sodium and chloride ions (0.1 M). Coarse-grained water molecules omitted for clarity. In (a), lipid tails are shown as while/purple lines, counter ions and coarse-grained water molecules are omitted for clarity. (c) Final snapshot after 52.5 ns of an all-atom simulation of PAH deposition on a citrate-AuNP. Counterions are omitted for clarity. See also Supplementary Note 4 and Figures S6 – S12.

Figure 5. PAH-wrapped nanoparticles alter bilayers in suspended vesicles, which then form sticky, macroscopic superstructures. (a) Normalized proton NMR spectra of (i) vesicles formed from a 9:1 mixture of DMPC:DMPG, (ii) PAH-AuNPs interacting with 9:1 DMPC:DMPG vesicles, (iii) PAH-AuNPs alone, and (iv) unbound PAH. The green dotted line tracks the chemical shift of the lipid headgroup protons; the blue, purple, and grey dotted lines track the chemical shifts of the PAH protons. All measurements made at 20 °C and in 0.1 M NaCl and at pH 7.4 (0.01 M Tris) in D₂O, for 12 nM vesicles and 10 nM particles after 2 h of incubation. z-Stack fluorescence image obtained from a glass surface in contact with a solution formed from mixing a 5 nM solution of PAH-wrapped 15-nm sized gold metal nanoparticles under conditions of 100 mM NaCl and 10 mM Tris buffer with a solution containing (b) 0.0625 mg/mL and (c) 0.00625 mg/mL vesicles (100 nm diameter) formed from a 9:1 mixture of DMPC:DMPG and 0.1% TopFluor-labeled PC. The liquid/solid boundary is visualized by the presence of micron-sized features and marked by the black rectangle in each image. Scale bars are 5 mm. See also Supplementary Note 5 and Figures S13 – S15.

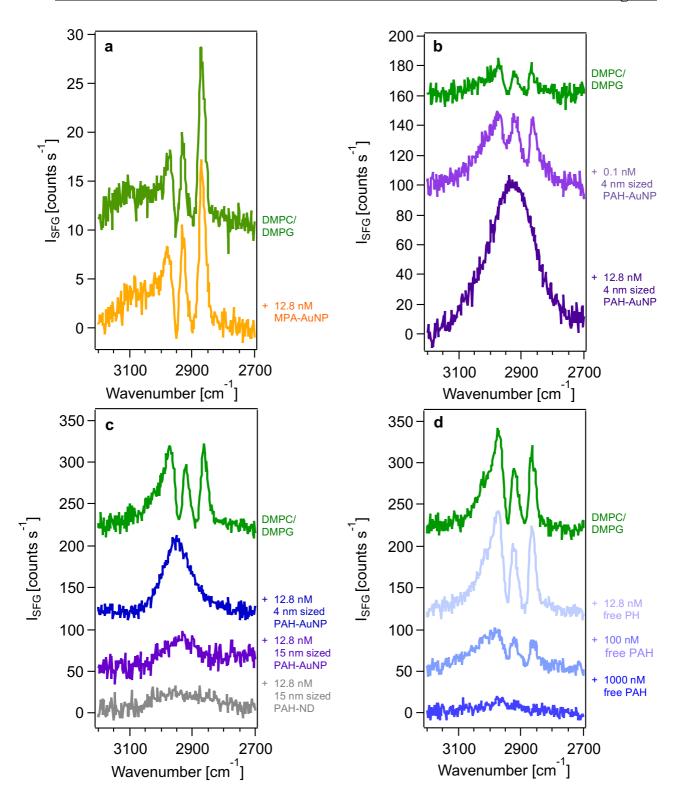


Fig. 1.

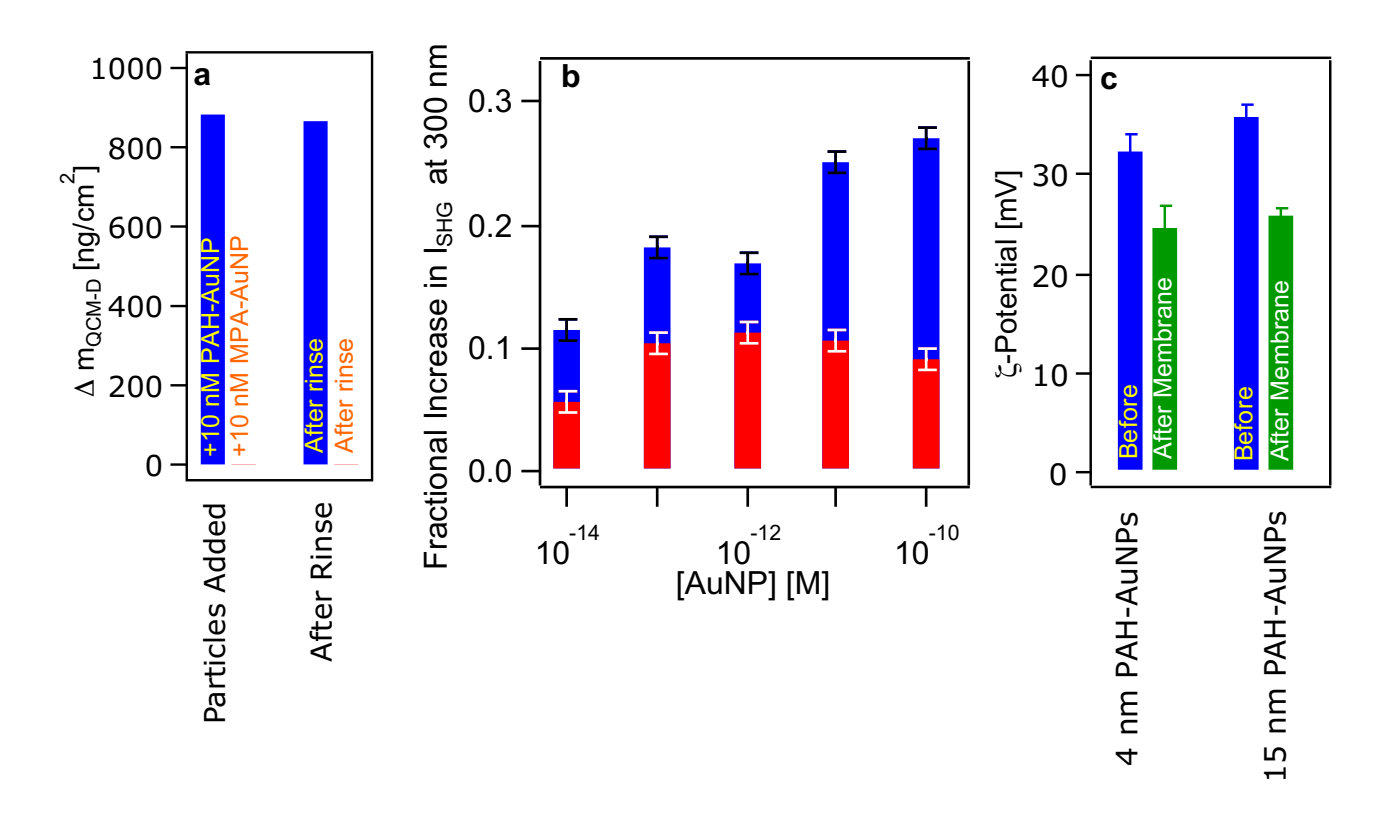


Fig. 2.

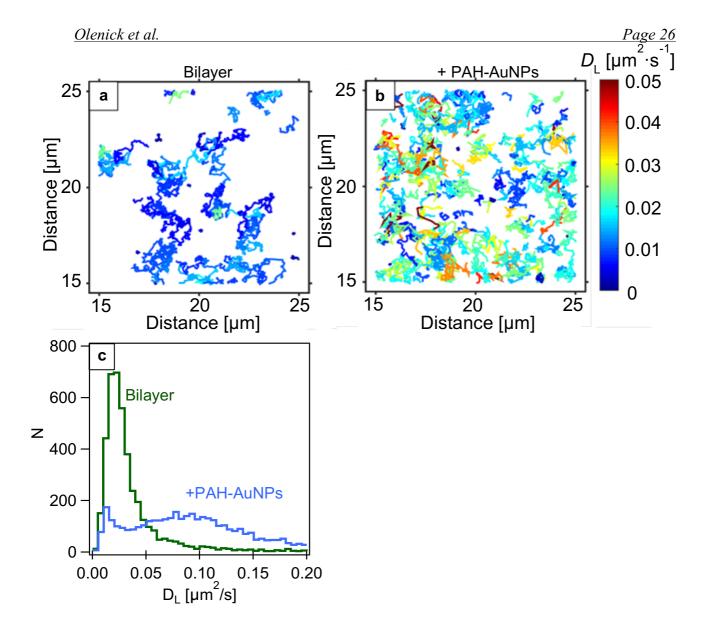


Fig. 3.

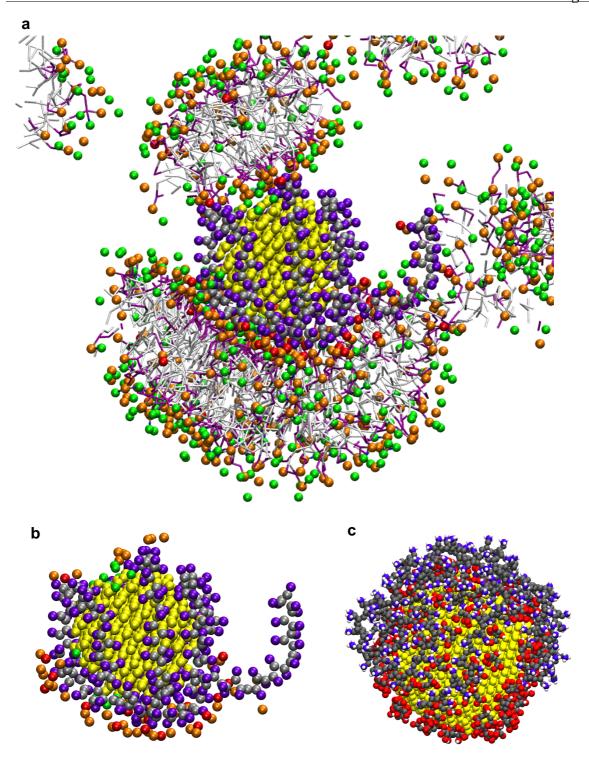


Fig. 4.

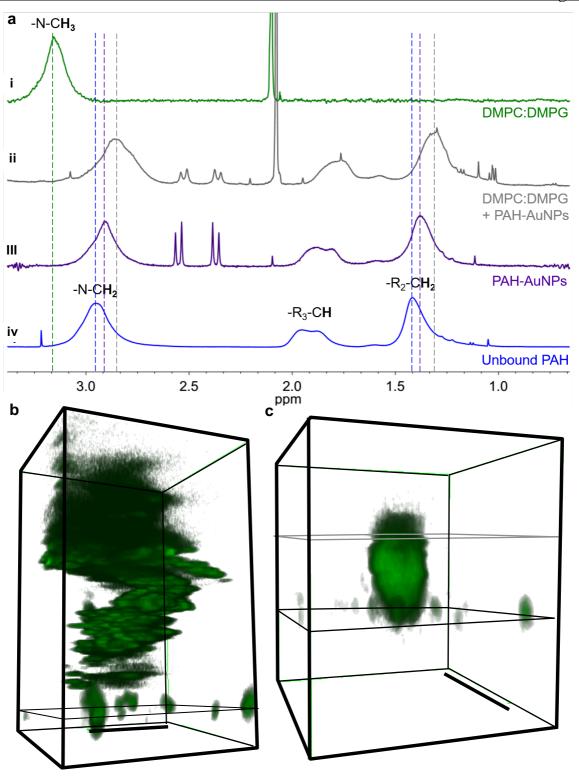


Fig. 5.

Table I. Experimental Outcomes ("+"=positive, "-"=negative) of Lipid Corona Formation.

Bilayer formed from	[NaCl] [mM]	4nm MPA- AuNPs	4nm PAH- AuNPs	15nm PAH- AuNPs	15nm PAH- ND	Free PAH Controls		
						PAH	PDADMAC	PVAM
100% DMPC	100	n.a.	(+)*	n.a.	n.a.	n.a.	n.a.	n.a.
9:1	1	n.a.	(+)*	n.a.	n.a.	n.a.	n.a.	n.a.
DMPC:DMPG	100	(-)* ^{#^}	(+)* ^{&%#=^}	(+)*	(+)*	(-) ^{\$#} (+) [@]	(-) ^{\$} (+) [@]	(-) ^{\$} (+) [@]
9:1 DOPC:DOTAP	100	(-) [§]	(-)#	n.a.	n.a.	n.a.	n.a.	n.a.
100% DOPC or POPC	100	(-)*	n.a.	n.a.	n.a.	n.a.	n.a.	n.a.

All particle concentrations at 10 nM except where indicated. Outcome determined *by SFG; &by ¹H NMR; \$by QCM-D and ¹H NMR from ref. 29; %by molecular dynamics simulations; ^by QCM-D; \$by SFG for 10 nM PAH-equivalent concentration; @by SFG for 1 mM PAH-equivalent concentration; #by spinning disk confocal microscopy; *by QCM-D from ref. 30 and by QCM-D, SHG, and cell sorting from ref. 31; ¯by TEM.

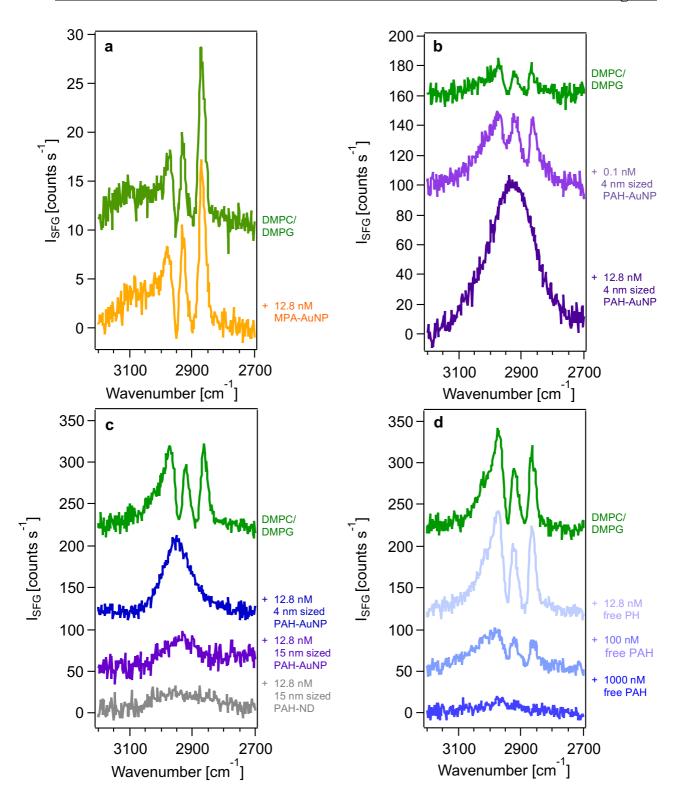


Fig. 1.

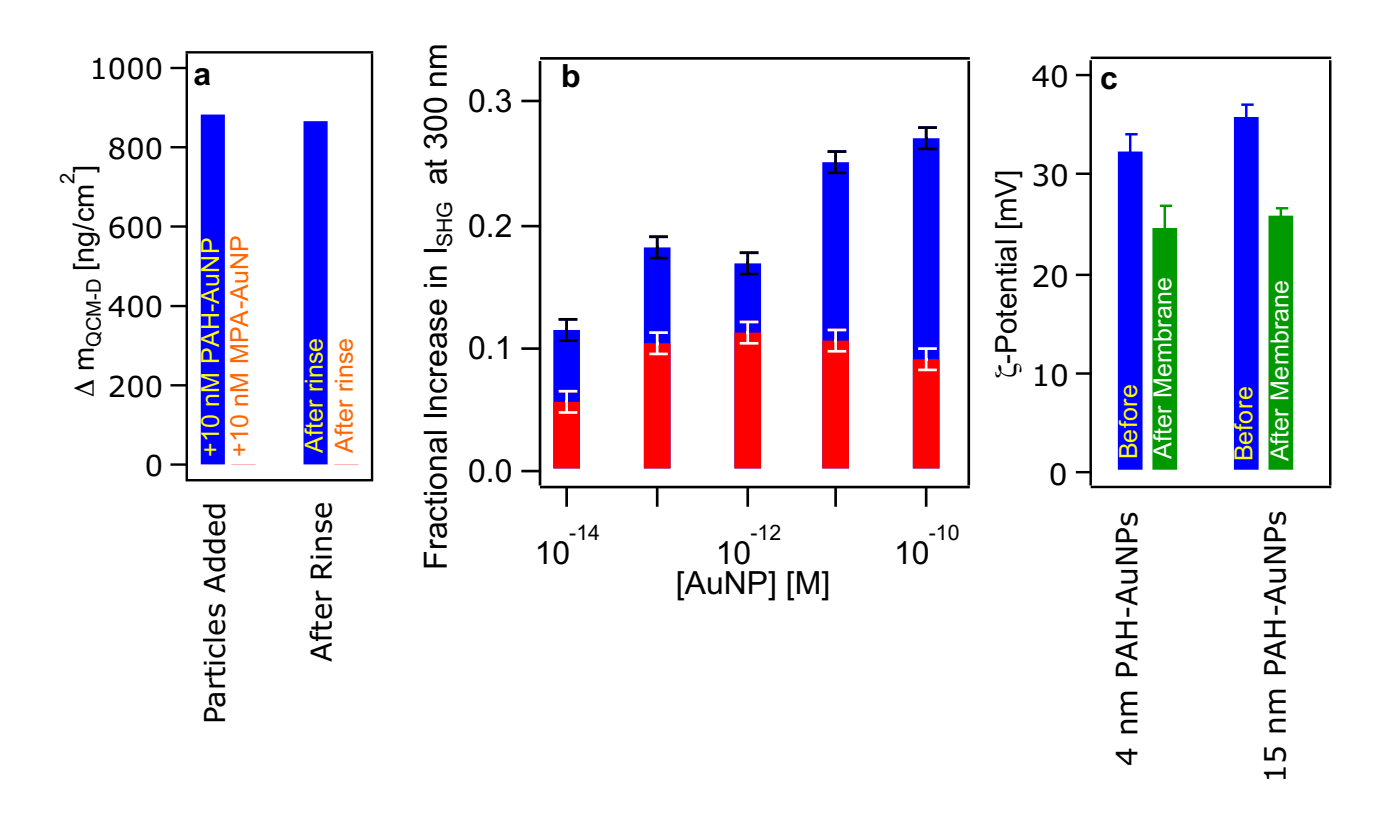


Fig. 2.

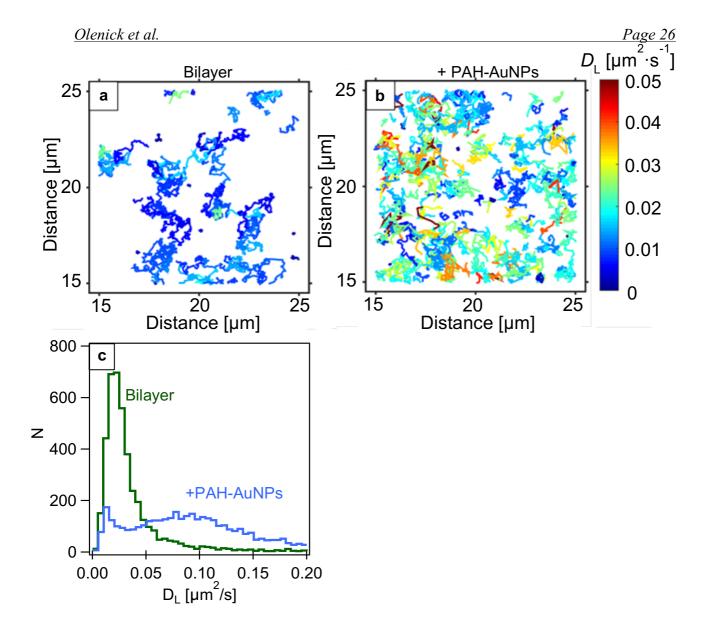


Fig. 3.

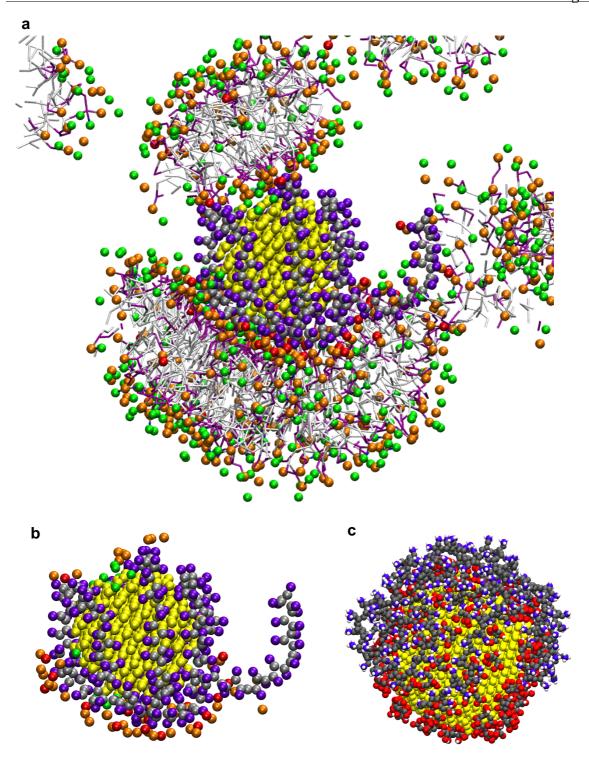


Fig. 4.

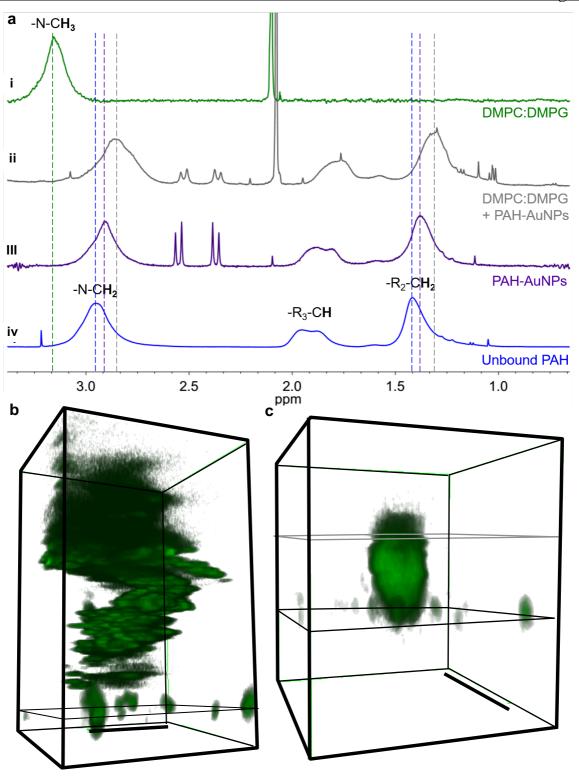


Fig. 5.